Chen *et al.*
Chinese Journal of Mechanical Engineering (2024) 37:66
https://doi.org/10.1186/s10033-024-01059-9

Chinese Journal of Mechanical Engineering

ORIGINAL ARTICLE

Open Access

Velocity-Incorporated Wear Model of Rolling Guide Shoe Material Selection

Longye Chen[1], Lingyu Yan[1], Chengliang Liu[1,2] and Zhinan Zhang[1,2*]

Abstract

To ensure an accurate selection of rolling guide shoe materials, an analysis of the intricate relationship between linear speed and wear is imperative. Finite element simulations and experimental measurements are employed to evaluate four distinct types of materials: polyurethane, rubber, polytetrafluoroethylene (PTFE), and nylon. The speed-index of each material is measured, serving as a preparation for subsequent analysis. Furthermore, the velocity-wear factor is determined, providing insights into the resilience and durability of the material across varying speeds. Additionally, a wear model tailored specifically for viscoelastic bodies is explored, which is pivotal in understanding the wear mechanisms within the material. Leveraging this model, wear predictions are made under higher speed conditions, facilitating the choice of material for rolling guide shoes. To validate the accuracy of the model, the predicted degree of wear is compared with experimental data, ensuring its alignment with both theoretical principles and real-world performance. This comprehensive analysis has verified the effectiveness of the model in the selection of materials under high-speed conditions, thereby offering confidence in its reliability and ensuring optimal performance.

Keywords Archard model, Wear model, Speed-index, Wear prediction

1 Introduction

Distinct from sliding guide shoes, which utilize metal as the material of contact with the guide rail, rolling guide shoes employ polymers. This polymeric material effectively minimizes friction between the guide shoe and guide rail while also imparting a damping effect to the elevator. Consequently, rolling guide shoes have garnered increasing attention in practical applications, surpassing sliding guide shoes. Nevertheless, the superior benefits of rolling guide shoes are intimately tied to the specific polymer utilized, as the properties of different polymers can significantly impact the performance of the roller. Therefore, thoroughly exploring the relationship between contact and friction among various polymers as potential guide shoe materials is crucial for assessing the suitability of rolling guide shoes in diverse application scenarios.

In Refs. [1–6] on rolling guide shoes, significant attention has been paid to their dynamic behavior and shock absorption capabilities. For instance, a three-dimensional rolling contact model was established to investigate the interactions between the rolling guide shoe and the guide rail [1]. This model derived contact stiffness coefficients in various directions, including normal, longitudinal, and horizontal, and calculated forces such as the normal Hertz force and tangential creep force within the contact area. Additionally, a nonlinear approach was proposed to enhance the accuracy of elevator car vibration models and assess the impact of uncertainty factors on the vibration response [2]. Furthermore, a mixed H_2/H_∞ optimal guaranteed cost state feedback control strategy was developed to mitigate horizontal vibrations resulting from friction and wear between the rolling guide shoe and the guide rail [3]. Similar research efforts have also been reported in Refs. [4–6].

*Correspondence:
Zhinan Zhang
zhinanz@sjtu.edu.cn
[1] School of Mechanical Engineering, Shanghai Jiao Tong University, Shanghai 200240, China
[2] State Key Laboratory of Mechanical System and Vibration, Shanghai Jiao Tong University, Shanghai 200240, China

However, the tribological properties between the guide shoe and the guide rail have received limited attention. Specifically, research is scarce on the wear of guide shoe materials under various operating conditions. Given that friction between these components can potentially cause damage and lead to failure, it is imperative to investigate the tribological characteristics of their interaction. Therefore, a comprehensive understanding of the tribological properties between the guide shoe and the guide rail, particularly the wear behavior of the former, is crucial for enhancing the performance and durability of rolling guide shoes.

The majority of prior wear prediction studies have relied heavily on the Archard wear model, which primarily emphasizes wear coefficients of various materials while overlooking the significant impact of pressure and velocity on material wear. For instance, ball-in-plane tests were conducted to investigate tribologically transformed structures and modify the hardness component of the Archard model [7]. Additionally, the Archard theory was broadened from dry contact scenarios to mixed lubrication conditions [8]. In another research, the Archard model was integrated with a spatial statistical approach, leading to a novel numerical algorithm for die wear depth estimation [9, 10]. A wear life model was also developed specifically for slippers in liquid friction applications, taking into account the permissible extent of wear [11, 12].

Notwithstanding the advancements made in wear prediction studies, there remains a significant gap in understanding the tribological properties of rolling guide shoes, particularly the intricate interplay between pressure and velocity on material wear. Given the critical importance of accurate wear prediction in ensuring the durability and performance of rolling guide shoes, it is imperative to investigate this area further. Future research efforts must, therefore, be directed toward developing rigorous and comprehensive wear prediction models that take into account the complex interactions between material properties, pressure, and velocity. By doing so, a deeper understanding of wear mechanisms can be gained and, ultimately, optimize the design and performance of rolling guide shoes.

In the revised Archard model [13], two crucial indices are introduced: the speed-index and the pressure-index. The speed-index specifically quantifies the sensitivity of the wear rate to changes in velocity. At low relative velocities, the impact of the speed-index on the wear rate is minimal. However, as the relative velocity increases, the wear rate rises geometrically, leading to significant wear in a relatively short period of time. This rapid wear can ultimately result in damage to the guide shoe, emphasizing the critical role of velocity in wear prediction and prevention.

For the shoe materials, polyurethane, rubber, polytetrafluoroethylene (PTFE), and nylon are among the established and potential materials used. Research efforts on these materials have primarily centered on analyzing and enhancing their wear characteristics after exposure to various operating conditions. In the case of polyurethane, investigators have delved into the impact of various solvents, nanoparticle concentrations, and annealing temperatures on the morphology and wear resistance of nano-polyurethane particle films [14]. Additionally, alumina particle-reinforced polyurethane matrix composites have been developed to bolster the wear resistance of polyurethane elastomers under erosive conditions [15]. Furthermore, the influence of different molecular weights on the scratch wear and abrasive wear behavior of three thermoplastic polyurethane elastomers has been explored [16]. Notably, it was discovered that higher molecular weights correlate with improved scratch resistance, crack resistance, and reduced abrasive wear volume loss. These findings provide valuable information for optimizing the selection and design of guide shoe materials to enhance their durability.

In addition to the aforementioned research, studying rubber wear has been a focal point in material science. A wear model was constructed, leveraging stress-strain relationships and stress-to-failure cycle estimations at high strain rates [17]. Furthermore, the nitrile rubber/short carbon fiber (NBR/SCF) composite was developed, and its friction and wear properties were thoroughly investigated [18]. Similarly, graphene–silicone rubber composites were prepared, and their mechanical properties and friction characteristics were examined [19]. Comparable studies have also been conducted on polytetrafluoroethylene (PTFE) [20–22] and nylon [23–25].

Despite the crucial importance of elucidating the relationship between wear and speed for a comprehensive wear analysis of rolling guide shoe materials, there is a conspicuous dearth of research exploring this relationship in the literature pertaining to both existing and potential guide shoe materials. This significant knowledge gap underscores the urgent need for further investigation in this domain to deepen the understanding of wear mechanisms and optimize the performance of these materials.

Compared to low-speed operation conditions, the rolling guide shoe experiences significantly greater wear under high-speed conditions. However, the current wear model for viscoelastic materials used in rolling guide shoes is inadequate in addressing this aspect, and the actual relationship between velocity and wear remains to be established. Exploring the relationship between speed and wear, as well as developing a more comprehensive wear model for viscoelastic materials in rolling

guide shoes at high speeds, is hence of utmost importance. The insights gained from such research could provide valuable guidance for material selection and scheduling replacement of rolling guide shoes, ensuring their optimal performance and durability in high-speed applications.

To investigate the intricate relationship between speed and wear, four existing or potential guide shoe materials (polyurethane, rubber, PTFE, and nylon) were experimentally analyzed and utilized in the development of a more precise wear model for viscoelastic materials. This comprehensive approach involved considering various factors such as wear duration, speed, and the mass of the materials before and after the test. Additionally, the rolling friction wear between these four materials and the guide rail material, Q235 steel, is meticulously quantified. Based on the experimental results, the speed-index and velocity-wear factor are derived for each material. These parameters provide critical insights into the wear behavior of the materials at different speeds. Furthermore, finite element analysis is employed to simulate the wear process, enabling a deeper understanding of the wear mechanisms involved. Utilizing the derived speed-index and velocity-wear factor, predictions are made regarding the wear of the materials at various speeds. This predictive capability is crucial for informing material selection and replacement scheduling decisions for rolling guide shoes. Overall, the findings of this study are expected to serve as a technical reference and provide theoretical support for the selection of guide shoe materials in diverse speed environments.

2 Experiment Method

2.1 Experiment Design

The experiment was conducted on a two-disk rolling–sliding wear test apparatus (JD-DRCF/M) situated at the East China Jiaotong University in Nanchang, Jiangxi Province, China. This sophisticated testing machine enables real-time user control over numerous parameters, including the duration of the test, the rotational speeds of the two test pieces, the positive pressure exerted between them, motor torque, and the displacement of the upper specimen, as detailed in Ref. [26]. Furthermore, it provides the flexibility to implement external temperature control, humidity control, and other operational conditions as per the specific requirements, as outlined in Ref. [27]. The experimental setup and its corresponding schematic diagram are presented in Figure 1.

In Figure 1, the parts of the testing machine consist of synchronous belt A, referred to as No.1; servo motor A, referred to as No.2; servo motor C, referred to as No.3; Q235 test piece, referred to as No.4; linear guide, referred to as No.5; load platform, referred to as No.6; synchronous belt B, referred to as No.7; torque sensor, referred to as No.8; rolling bearing, referred to as No.9; viscoelastic test piece, referred to as No.10; servo motor B, referred

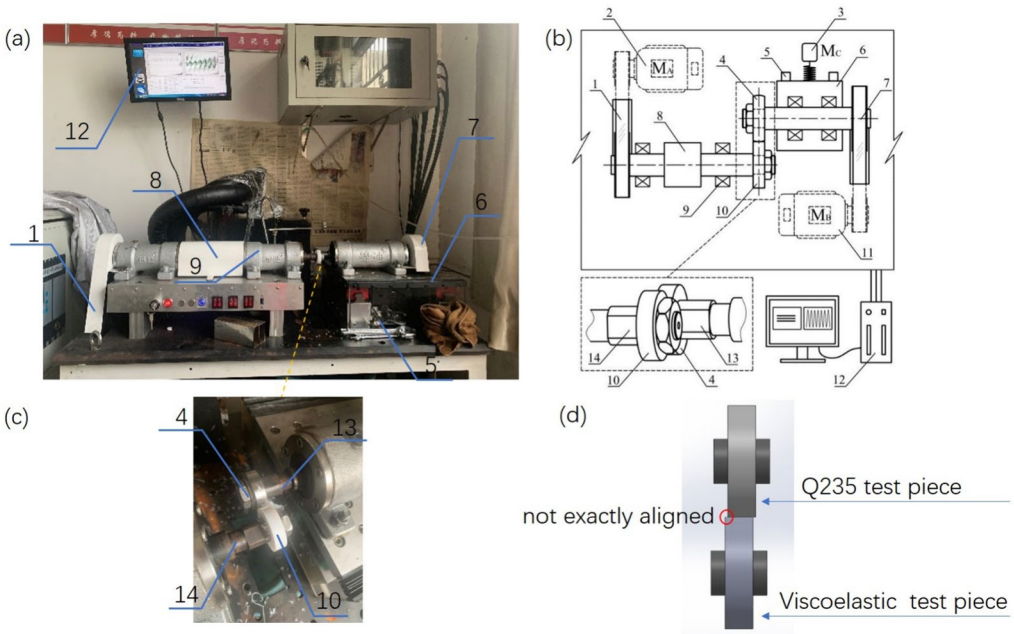

Figure 1 Experimental setups for wear measurements during the test process: (**a**) Stepless speed-regulating wheel-rail rolling contact fatigue testing machine, (**b**) Schematic for stepless speed-regulating wheel-rail rolling contact fatigue testing machine [28], (**c**) Close-up of test process and test piece, (**d**) Misaligned 3D model for wear simulation

to as No.11; data acquisition and control system, referred to as No.12; rotation axis B, referred to as No.13; rotation axis A, referred to as No.14 [28]. Test pieces are cylindrical rings with outer diameter $D = 40$ mm, inner diameter $d = 16$ mm, and height $H = 10$ mm. The upper test piece (Q235 test piece, Part 4) and the lower test piece (viscoelastic test piece, Part 10) are driven by servo motor A (Part 2) and servo motor B (Part 11). The load between two test pieces is applied by servo motor C (Part 3). The distance between the upper rotation axis (Part 13) and the lower rotation axis (Part 14) is adjustable according to the change of the positive pressure so as to ensure that positive pressure is kept constant. The loading platform (Part 6) with the upper test piece on it slides on the linear guide (Part 5). All setups can be implemented from the data acquisition and control system (Part 12). These include speed, load, and test duration.

The test pieces were securely installed on the lower sample, whereas a Q235 steel test piece was precisely mounted on the upper sample. The motor speed was carefully adjusted to align with the desired linear speed of the test piece, and the positive pressure of the sample was set to ensure constant contact stress throughout the experiment. The experiment duration was established as 1800 s, with a pre-determined slip of 0.2. Each material was subjected to rigorous testing under three distinct speed conditions, followed by a verification experiment conducted at a higher speed. Specifically, the linear speeds for the three test speed settings were set at 0.5 m/s, 1 m/s, and 1.5 m/s, respectively. For the verification experiment, the linear speed was increased to 2 m/s. Each material-speed combination was tested three times to guarantee reproducibility and consistency of the results. It is noteworthy that due to inevitable size deviations, the viscoelastic test piece and the Q235 test piece were not perfectly aligned. This misalignment is a crucial factor that must be taken into account during the simulation process, as clearly demonstrated in Figure 1(d).

2.2 Experiment Materials

The experimental materials selected are polyurethane, rubber, PTFE, and nylon. The four materials are in rolling contact with the guide rail material Q235 steel, respectively. Table 1 shows the material properties of the four materials obtained by measurement and the material properties of Q235.

2.3 Experiment Procedure

The experiment procedure consists of five steps, and the flow chart is shown in Figure 2.

Step 1: Before the experiment, use an ultrasonic cleaner with ethyl alcohol for 5 min to clean the surface of the test piece to remove surface stains.

Table 1 Material properties

Material	Polyurethane	Rubber	PTFE	Nylon	Q235
Density (kg/m^3)	1042.57	1697.33	2168.81	943.72	7850
Young's modulus (MPa)	20.58	10.89	377.64	544.33	210000
Poisson ratio	0.42	0.47	0.46	0.42	0.25

Step 2: After the test piece is dried, weigh the test piece and record the mass as the pre-experiment mass.

Step 3: Conduct the experiment as described in Section 2.1 and record the data. The data, such as friction torque, positive pressure, and time, are collected in real time. The real-time coefficient of friction during the experiment can be calculated.

Step 4: After the experiment, use the ultrasonic cleaner with ethyl alcohol again to clean the surface of the test piece to remove residues on the surface, and weigh it after drying to obtain the mass after the experiment. Thus, the wear amount can be calculated by the pre-experiment mass minus the post.

Step 5: Use a three-dimensional morphometer to measure the surface of the test piece.

3 Wear Model

3.1 Archard Wear Model

The generally accepted model for predicting wear is the Archard wear model

$$\mathrm{d}W/\mathrm{d}t = KpV/H, \tag{1}$$

where $\mathrm{d}W/\mathrm{d}t$ is the wear amount per unit time, K is the wear coefficient, p is the positive pressure, V is the relative velocity, and H is the material hardness of the worn material.

It is found that the wear rate is proportional to the index of the positive pressure, and the index varies depending on the two contact materials [29]. The pressure and speed-index for the ASTM A109 steel and SAE 1010 steel tribopair had been used to perform lifetime prediction experiments [30]. Here, we assume that the modified Archard wear model for the tribopair of rolling guide shoe could be applied [13]:

$$\mathrm{d}W/\mathrm{d}t = K'p^m V^n/H, \tag{2}$$

where K' is wear coefficient for the modified model, m is pressure-index, and n is speed-index. Table 2 shows various application scenarios of the Archard wear model.

The materials of previous studies [9, 30–34] using the Archard model are mainly metals or metal compounds. Furthermore, most of them use the basic Archard wear model, while the modified Archard model was only

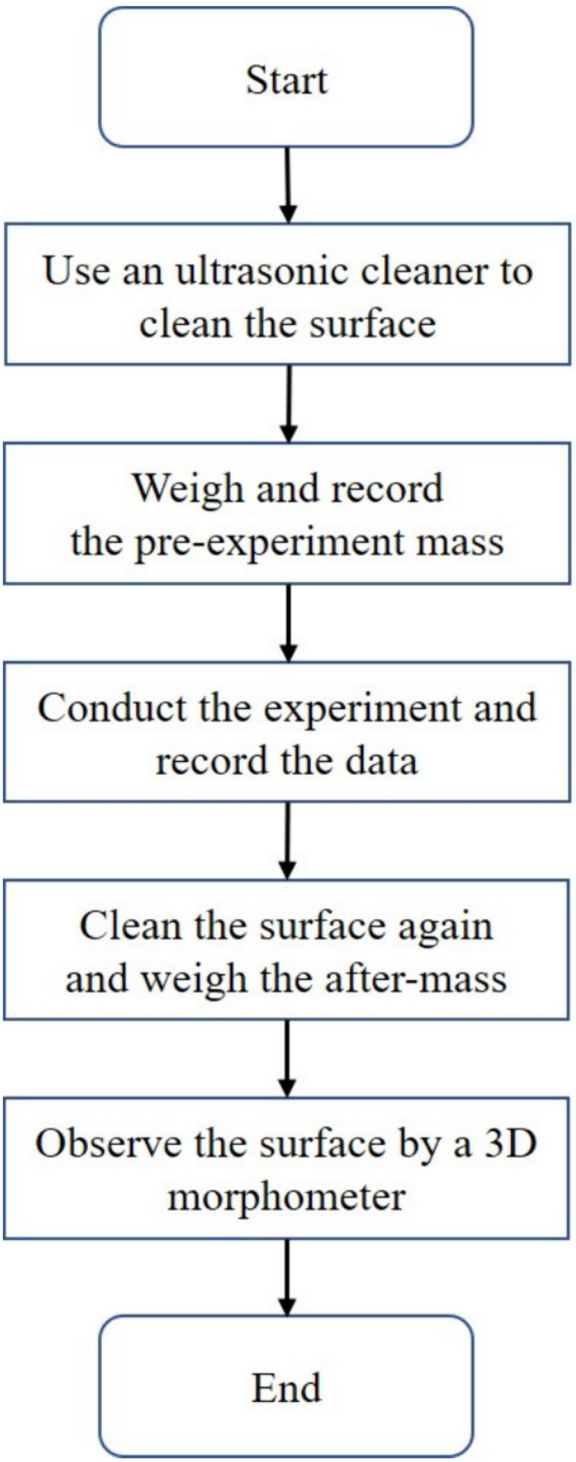

Figure 2 The flow chart for the five steps of the experiment procedure

used to study wear between different steels [30]. Therefore, the wear model of viscoelastic materials needs further exploration. To examine the relationship between wear and speed for viscoelastic materials, it is necessary to experimentally measure whether the speed-index (n in Eq. (2)) is unity or not.

3.2 Wear Prediction

Step 1: Measure the wear amount of the same material at different speeds under constant pressure and process the wear mass to eliminate the error existing in the sample itself. It is the product of the wear percentage of a single sample and the mass of the standard part. That is

$$\overline{w} = \rho(w/M)\left[\pi(D-d)^2 H/4\right], \tag{3}$$

where $\overline{w}$ is the ideal wear mass, w is the experimental wear mass, M is the original mass of the test piece, D is the outer diameter of the test piece, and H is the height of the test piece minus the dislocation distance of the upper and lower samples.

Step 2: Linearly fit the logarithm of the wear amount and the logarithm of the relative velocity in the experiment. Thus, the slope of the fitted straight line is the corresponding speed-index n. Furthermore, obtain the velocity-wear factor

$$k = \Delta M/\left(\rho t p\, \Delta v^n\right), \tag{4}$$

where ΔM is the experimental wear amount, ρ is the material density, t is the experimental time, p is the normal pressure, Δv is the relative speed, and n is the speed-index.

Step 3: Assume that the pressure-index is unity, simulate the experimental process on Ansys workbench.

Step 4: The higher speed wear amount is predicted. The logarithm of the ideal wear amount and the relative velocity are further fit onto a straight line. That is

$$\begin{cases} \ln\left(\widetilde{\Delta w}\right) = n\ln V + b, \\ \widetilde{\Delta w} = \exp\left(n\ln V + b\right), \end{cases} \tag{5}$$

$$\eta = \widetilde{\Delta w}/\overline{w} \times 100\%, \tag{6}$$

where $\widetilde{\Delta w}$ is the predicted wear amount, n is the speed-index, b is the intercept of the speed-index plot, η is the relative error, and $\overline{w}$ is the ideal experimental wear amount. The overall process is shown in Figure 3. It can be concluded as: obtaining data from experiments at different speeds; calculating the speed-index and wear factor from data for the first three speeds; simulating wear according to the speed-index and wear factor; making wear predictions; and calculating error by both theory and simulation.

Table 2 Archard model used in previous literature [9, 30–34] and our work

Scholar (year)	Wear material	Abrasive material	Wear model
Liu et al. (2022) [9]	Wheel	Rail	$V_w = KNd/H$
Akama et al. (2020) [31]	Wheel steel	Rail steel	$V = KNd_s/H$
Ramalho et al. (2013) [32]	AISI 4140	AISI 1055	$V = K_c Nx/H$
Khader et al. (2012) [33]	Silicon nitride	100Cr6	$V_w = C_0 F_N s$
Kim et al. (2019) [30]	ASTM A109 steel	SAE 1010 steel	$\delta = kP^a N^b$
Zhou et al. (2021) [34]	Rail	Carriage	$W = KQ\|V\|\Delta t$
Our work	Polyurethane etc.	Q235	$dW/dt = K' p^m V^n/H$

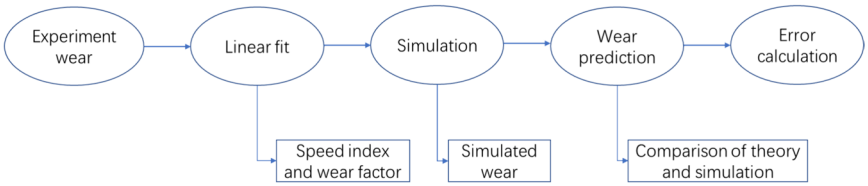

Figure 3 Logic diagram to summarize the process

3.3 Wear Simulation Process

When simulating the wear process of polyurethane with the linear speed 1 m/s, the CAD model is designed according to the tribopair. The connection between the tribopair is set to be frictional with the experimentally measured coefficient of friction. In the frictional contact, the commands (APDL) for wear are inserted to use the built-in wear model. The mesh size for polyurethane is set to 0.2 mm, and that of the other parts is set to 2.5 mm. For the boundary conditions, set the rotation shaft of Q235 to be fixed, set the rotational velocity of the polyurethane test piece to 50 rad/s and that of the Q235 test piece to 60 rad/s, set a frictionless support on the side faces of the two test pieces, and set a force on the rotation shaft of polyurethane pointing to the rotation shaft of Q235 with the value 30 N. The force and the rotational velocities are placed on two joints. The first one is a body-ground general joint on polyurethane, where the force and the rotational velocity are set. The other one is a body-ground revolute joint on Q235, where the rotational velocity is set. In the analysis settings, the minimum and maximum substeps are set to 10 and 1000, and the initial sub-steps are 100. Meanwhile, large deflection is activated. After the boundary condition and the analysis are set, carry on the wear simulation and record the wear data.

4 Results and Discussion

4.1 Test Results

The experiment on each material with each speed is conducted three times, and the results are the average of the wear mass of the three test pieces under the same conditions. Each material was experimented with different line speeds, which are listed in the second column. The wear mass in the third column is obtained from the mass difference before and after the test weighed by an electronic balance, and the ideal wear mass in the last column is calculated according to Eq. (3). The experimental results of each material with each speed are listed in Table 3.

4.2 Data Processing and Discussion

4.2.1 Speed-index

As for the experimental settings, the slip is 0.2 and the relative velocities are 0.1 m/s, 0.2 m/s, and 0.3 m/s, respectively. By taking the logarithm of the ideal wear amount and the relative velocity, the fitted straight lines are shown in Figure 4. The lines are obtained by fitting the line of the logarithm of ideal wear mass and the logarithm of relative speed: each fitting line's slope represents the corresponding material's speed-index.

According to the fitted line, the speed-index of polyurethane, rubber, PTFE, and nylon can be obtained as

Table 3 Experiment results

	Line speed (m/s)	Wear mass (g)	Ideal wear mass (g)
Polyurethane			
Sample1	0.5	0.0537	0.0530
Sample2	1.0	0.0667	0.0684
Sample3	1.5	0.1031	0.1022
Sample4	2.0	0.1174	0.1168
Rubber			
Sample1	0.5	0.0024	0.0025
Sample2	1.0	0.0426	0.0435
Sample3	1.5	0.0627	0.0638
Sample4	2.0	0.2390	0.2397
PTFE			
Sample1	0.5	0.0365	0.0365
Sample2	1.0	0.1398	0.1410
Sample3	1.5	0.2264	0.2277
Sample4	2.0	0.4248	0.4232
Nylon			
Sample1	0.5	0.0036	0.0036
Sample2	1.0	0.0046	0.0046
Sample3	1.5	0.0052	0.0052
Sample4	2.0	0.0056	0.0056

0.5735, 3.0918, 1.6966, and 0.3338, respectively. The results in Table 4 show that the speed-index of polyurethane and nylon is smaller than one while the speed-index of PTFE and rubber is greater than one. This indicates that the wear of polyurethane and nylon is relatively insensitive to speed changes, while the wear of PTFE and rubber is more sensitive to speed changes. As the speed continues to increase, the wear amount of PTFE and rubber increases faster than that of polyurethane and nylon. Therefore, in relatively low-speed elevators where the impact of running speed on the wear of guide shoe materials is limited, rubber is more commonly used as guide shoe material due to its low price. Meanwhile, polyurethane is used more in medium- and high-speed elevators despite its relatively higher cost than rubber.

4.2.2 Velocity-wear Factor k

According to Eq. (4), the velocity-wear factor (representing the absolute wear amount of wear) for each tribopair and the average velocity-wear factor for each material is obtained. The velocity-wear factor k and the speed-index n of the four materials are shown in Table 4.

The results clearly indicate that the velocity-wear factor varies significantly among different materials, differing by several orders of magnitude. Specifically, nylon exhibits the lowest wear rate, followed by polyurethane and PTFE,

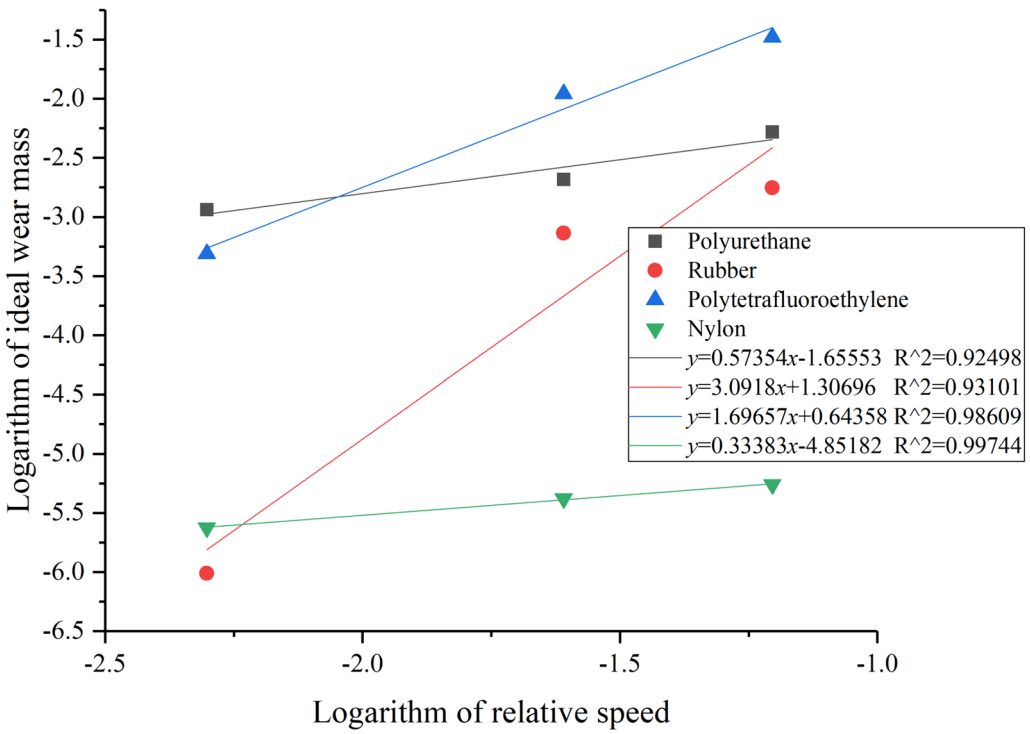

Figure 4 Speed-index of the four materials

Table 4 Speed-index and velocity-wear factor of the four materials

Material	Polyurethane	Rubber	PTFE	Nylon
Speed-index	0.5735	3.0918	1.6966	0.3338
Velocity-wear factor	3.2238×10^{-6}	4.3479×10^{-5}	2.6817×10^{-6}	3.0147×10^{-8}

while rubber has the highest wear rate. This implies that materials with a larger velocity-wear factor are more susceptible to friction-induced consumption when interacting with Q235 steel. Consequently, these materials are more prone to damage, potentially leading to permanent harm to the rolling guide shoe. Therefore, it is advisable to prioritize materials with a lower wear factor for use as rolling guide shoes. This choice will ensure greater durability and reliability in friction-prone applications.

4.2.3 Simulated Wear Amount

The 3D model utilized for the simulation is meticulously crafted based on the rolling friction test conducted on the two test pieces, as depicted in Figure 1(d). Within the simulation, crucial parameters such as the coefficient of friction for each tribopair (determined by torque and normal pressure), the actual speed difference, the normal pressure, and the contact misalignment of the test pieces are precisely set. Additionally, the wear command is configured according to the speed-index and velocity-wear factor obtained from Table 3. This ensures that the simulation accurately reflects the real-world conditions and factors influencing the rolling friction behavior of the test pieces.

During the 30-minute test, we observed three significant phenomena. Firstly, the friction pair and the friction conditions remained constant throughout the experiment. Secondly, upon close examination of the three-dimensional morphology after the test, we found that the wear type was exclusively adhesive wear, as detailed in Section 4.2. Lastly, the amount of wear incurred during the 30-minute test was insignificant compared to the overall size of the test piece, indicating that the shape remained virtually unchanged. Based on these observations, we can confidently conclude that the wear rate per unit time remained constant throughout the 30-minute duration of the experiment. Utilizing simulation techniques, we were able to determine the wear amount for a one-second interval, which allowed us to extrapolate the wear amount for the entire 30-minute period. Consequently, we set the simulation step size to one second to ensure accurate and precise results. The simulation outcomes are presented in Figures 5 and 6, providing a comprehensive understanding of the wear behavior under the given friction conditions.

Figure 5 summarizes the simulated wear volumes of various materials at different speeds. The simulation wear within 1 s presents a good linearity, which is consistent with the previous characteristics. Figure 6 only shows the number of contact elements of the four materials at the speed of 2 m/s. The differences in their respective number of contacts are caused by the different mesh sizes for various materials, the purpose of which is just to converge the results. Considering that the results under other conditions are remarkably similar, those results are listed in Figure 7. Figure 7(a) shows the number of contact elements of polyurethane at speeds of 0.5 m/s, 1 m/s, 1.5 m/s, and 6 m/s, respectively. Figure 7(b) shows the number of contact elements of PTFE at speeds of 0.5 m/s, 1 m/s, 1.5 m/s, and 6 m/s, respectively. Figures 7(c) and 7(d) show the number of contact elements of nylon and rubber at the same speeds above. The results of Figure 6 show that during the one-second simulation progress of four materials, the number of contact elements is kept unchanged, implying the unchanged shape. The results of Figures 5 and 6 further prove the feasibility of using unit time wear to predict thirty-minute wear. Then, we recorded the wear results of all working conditions and compared them with the test results to assess the error, as shown in Table 5.

It can be observed that significant discrepancies exist between the simulation outcomes and the experimental results obtained for rubber. Furthermore, it has been discovered that the velocity-wear factor of rubber varies significantly at different speeds. However, the mean value of these velocity-wear factors is utilized as input in the Ansys simulation. Consequently, this has led to a significant deviation in the results for the first three groups. On the other hand, the velocity-wear factor for the fourth group is closer to the mean value, leading to a smaller margin of error. Additionally, it is noteworthy that polyurethane, PTFE, and nylon, in contrast to rubber, exhibit a reduced level of error, with nylon demonstrating particularly accurate results. This implies that the wear behavior of these three materials can be more accurately predicted through simulation, especially at higher speeds.

4.2.4 Predicted Wear Amount

On the basis of the results in Table 4, conduct the wear prediction of experiments with unchanged positive pressure when the linear speed is 2 m/s. The predicted wear amount and the prediction error are listed in Table 6.

The errors may be caused by misalignment of the test piece. The two sides of the test pieces cannot be aligned due to the deformation of the test pieces of the four materials. According to the result of the stress simulation, larger stress indeed occurs at the contact edges. Such large stress may cause a large enough strain to have an

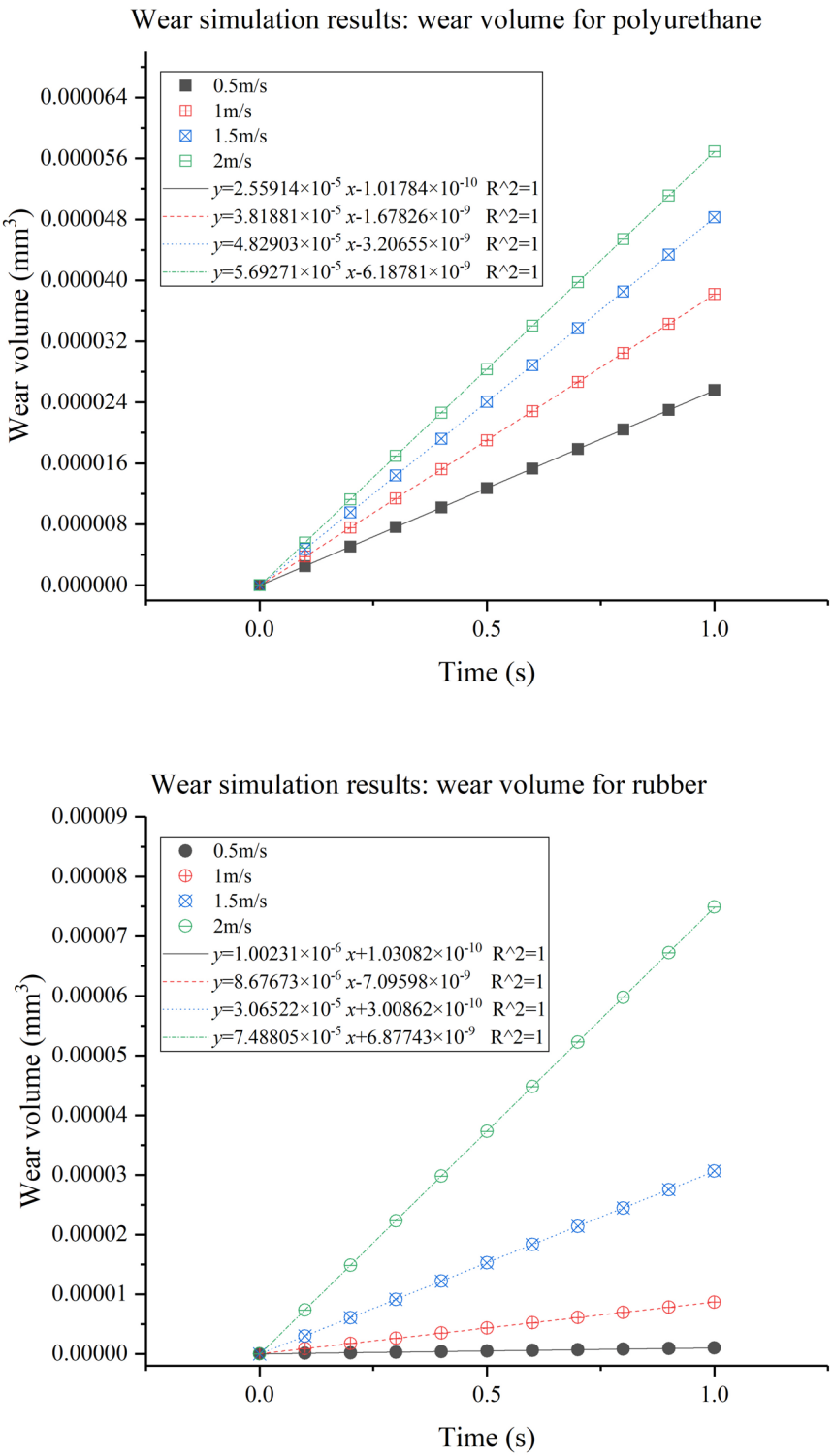

Figure 5 Wear simulation results: wear volume for polyurethane, rubber, PTFE, and nylon

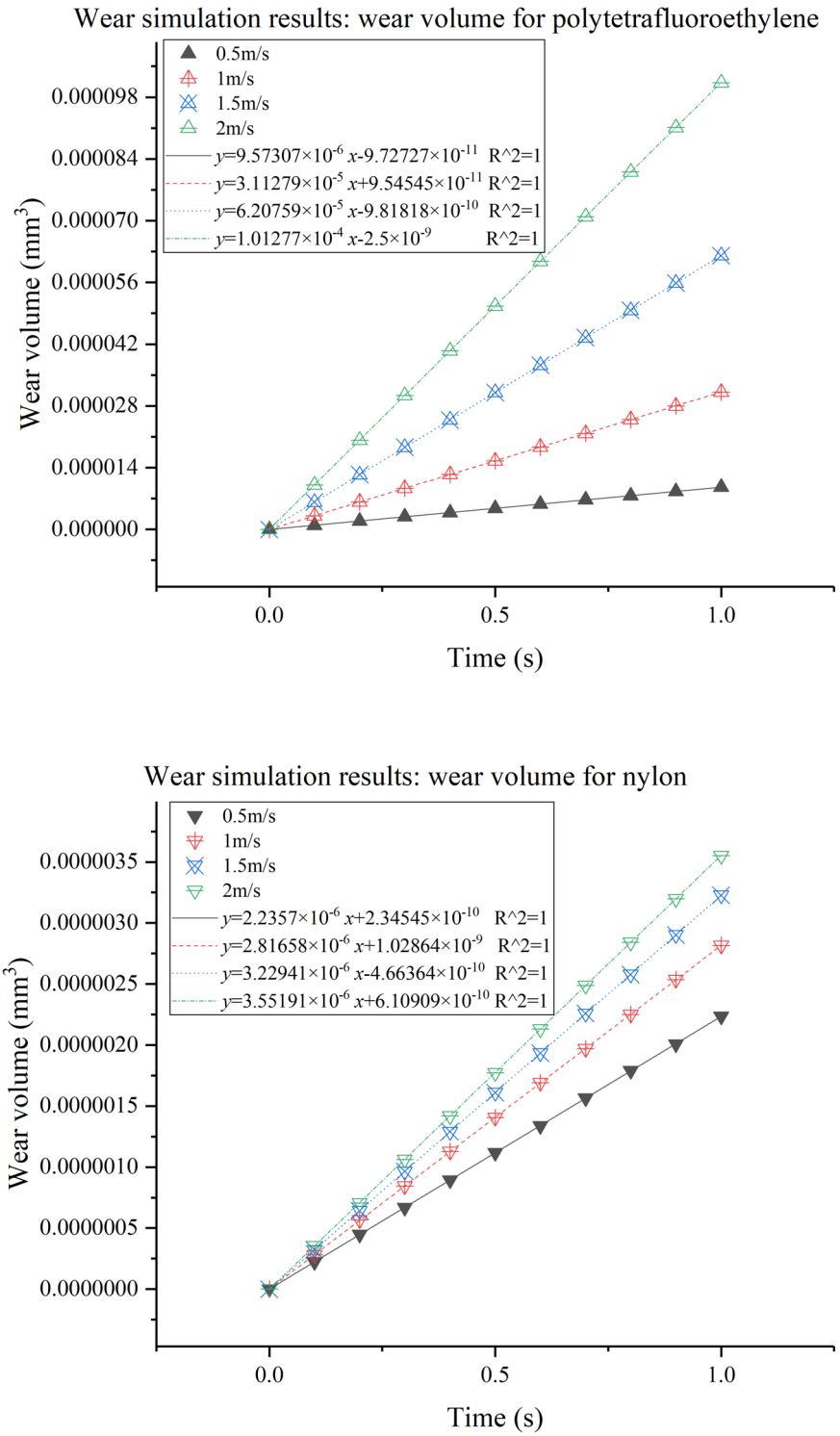

Figure 5 continued

inconstant Young's modulus, which can cause the error. Moreover, the prediction errors of the four materials are all within 10%, which can be used for wear predictions at higher speeds. Among them, the prediction errors of polyurethane, PTFE, and nylon are less than 5%, indicating a more effective prediction.

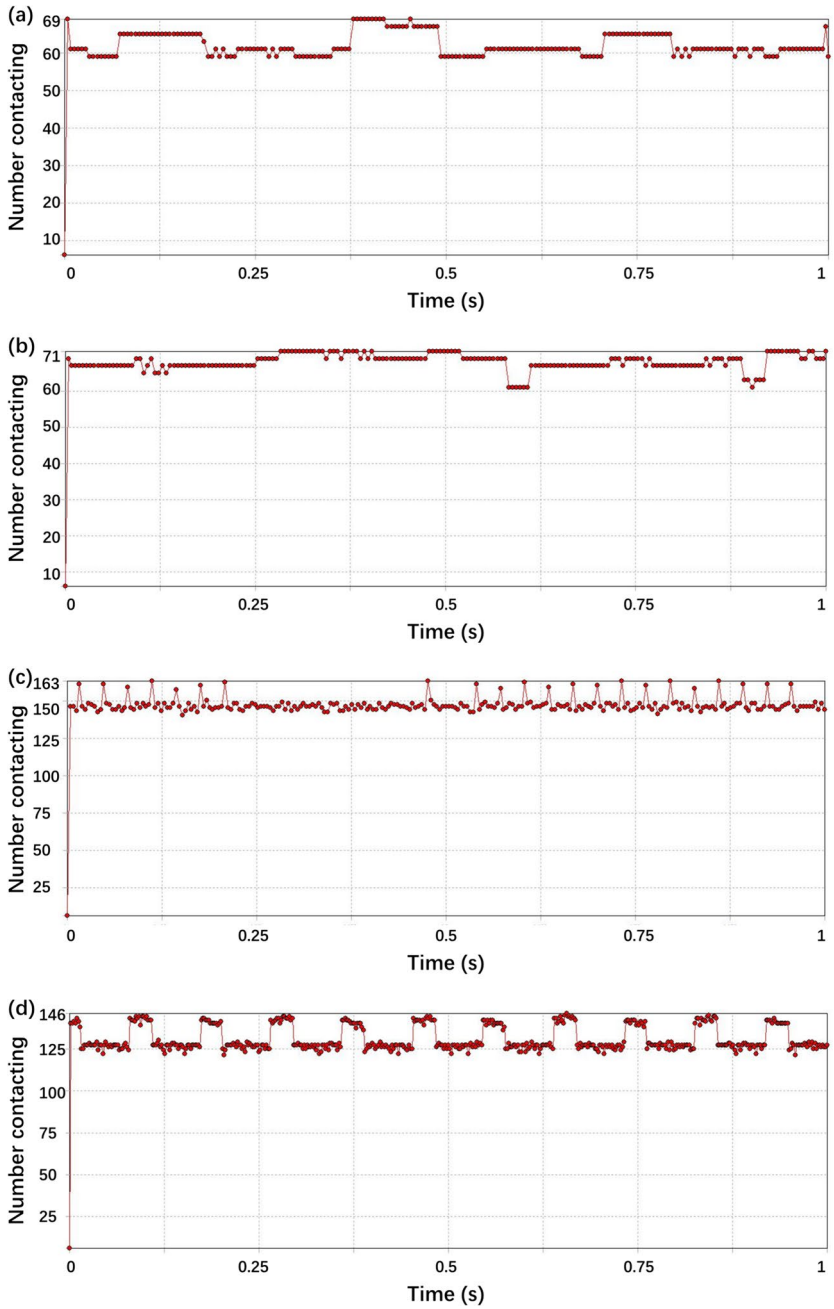

Figure 6 Simulation results: number contacting of 2 m/s for (**a**) polyurethane, (**b**) rubber, (**c**) PTFE, (**d**) nylon

The error of rubber and PTFE is larger than that of polyurethane and nylon, but the causes for the larger error of rubber and PTFE are different. For rubber, it is because its hardness is too small. During the experiment, due to the dislocation of the upper and lower samples, the rubber test piece was plastically deformed, which made the error larger. However, this is not the case for PTFE. The cause for the large error of PTFE is its small coefficient of friction. Such a small friction coefficient makes it unable to remain relatively stationary with the rotating shaft during the experiment, and slide relative to the shaft produces friction, resulting in additional wear at the contact between the test piece and the shaft. Such additional wear is also speed-dependent and leads to inaccurate predictions. The comparison of the theoretical prediction with the simulation results is presented in Table 7.

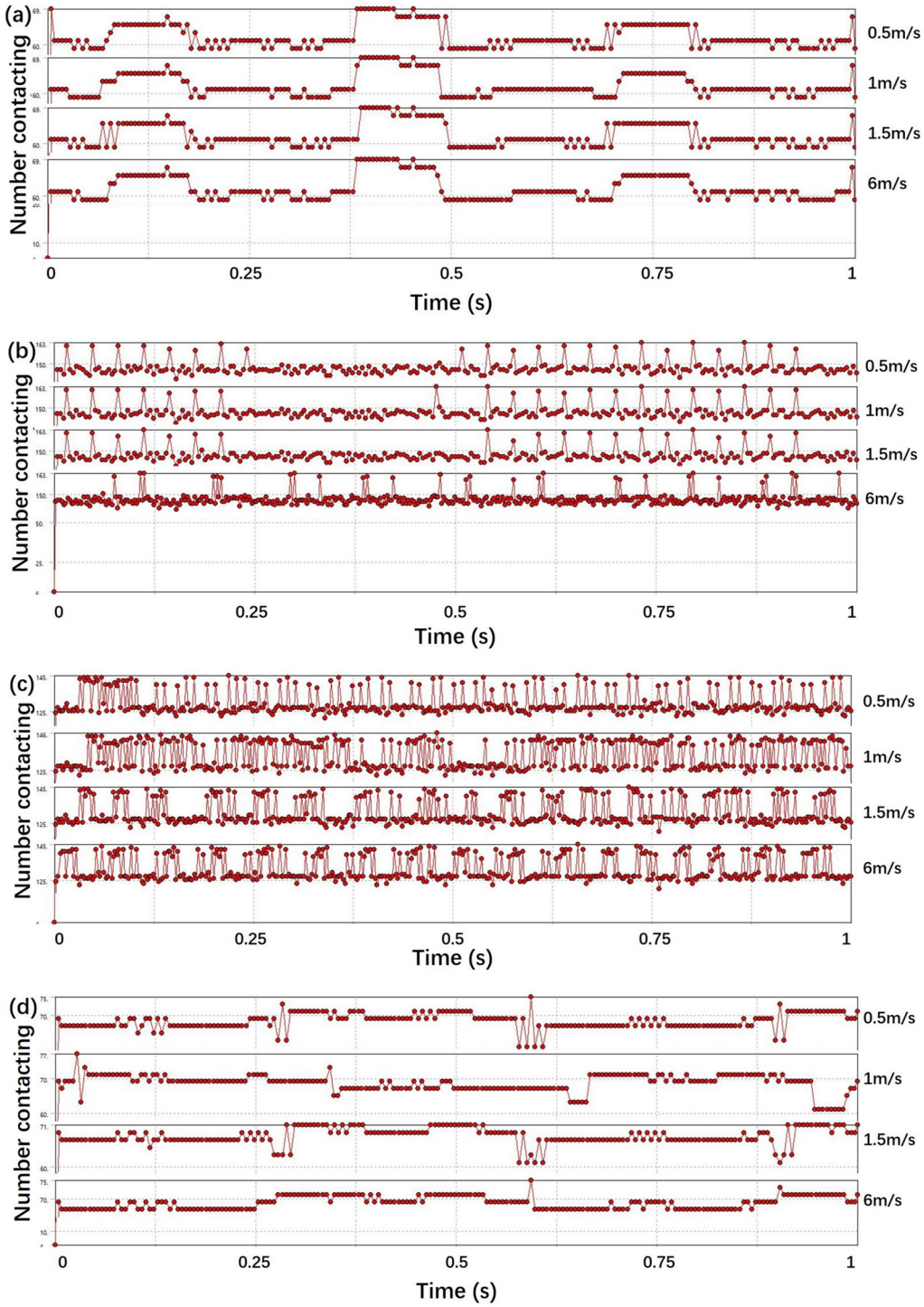

Figure 7 Simulation results: number contacting of 0.5 m/s, 1 m/s, 1.5 m/s, and 6 m/s for (**a**) polyurethane, (**b**) PTFE, (**c**) nylon, (**d**) rubber

There is a slight difference between the error of the theoretical results and the simulation results, which further proves the feasibility of using simulation to predict high-speed wear. However, in view of the variability of the velocity-wear factor of rubber, it is necessary to investigate further the influence of speed on the wear coefficient before using simulation to predict rubber wear.

Table 5 Comparison of experiment and simulated wear

	Line speed (m/s)	Ideal wear mass (g)	Simulated wear mass (g)	Error
Polyurethane				
Sample1	0.5	0.0530	0.0507	−4.34%
Sample2	1.0	0.0684	0.0756	10.53%
Sample3	1.5	0.1022	0.0956	−6.46%
Sample4	2.0	0.1168	0.1127	−3.51%
Rubber				
Sample1	0.5	0.0025	0.0031	24.00%
Sample2	1.0	0.0435	0.0265	−39.08%
Sample3	1.5	0.0638	0.0938	47.02%
Sample4	2.0	0.2397	0.2291	−4.42%
PTFE				
Sample1	0.5	0.0365	0.0379	3.84%
Sample2	1.0	0.1410	0.1233	−12.55%
Sample3	1.5	0.2277	0.2458	7.95%
Sample4	2.0	0.4232	0.4011	−5.22%
Nylon				
Sample1	0.5	0.0036	0.0036	0.00%
Sample2	1.0	0.0046	0.0046	0.00%
Sample3	1.5	0.0052	0.0052	0.00%
Sample4	2.0	0.0056	0.0058	3.57%

In addition, on the basis of the above results, four kinds of materials are simulated under the working condition of 6 m/s. Figure 8 shows the simulated wear amount under this working condition. The wear of the four materials within 1 sec under the working condition of 6 m/s is still linear, indicating that the above hypothesis is valid. At the same time, the wear amount of rubber is greater than that of PTFE and much greater than that of nylon and polyurethane. This is consistent with the theoretical prediction. Then, compared with the results of 2 m/s, the results in Figure 8 show that the increase in the wear amount of nylon and polyurethane is small, while the increase of rubber and PTFE is large. The results are consistent with the properties of the speed-index. Based on the above results, it is concluded that the wear of rubber and PTFE increases much more than that of polyurethane and nylon at higher speeds.

In Figures 5 and 7, the wear simulation results show that the volume of wear is directly proportional to the wear time. However, the amount of wear rate from the experiment. Therefore, it is not possible to judge whether this is the case in real-world situations. It is, however, conjectured that the direct proportionality is due to the smooth surface of the 3D model. However, the surface of the real test piece is not smooth enough, so the volume of wear may not be directly proportional to the wear duration.

Table 6 Wear prediction and error

Material	Polyurethane	Rubber	PTFE	Nylon
Predicted wear amount (g)	0.1129	0.2174	0.4021	0.0058
Ideal wear amount (g)	0.1168	0.2397	0.4232	0.0056
Error	−3.32%	−9.30%	−4.99%	3.57%

Table 7 Comparison of theory and simulation

Material	Polyurethane	Rubber	PTFE	Nylon
Ideal wear amount (g)	0.1168	0.2397	0.4232	0.0056
Predicted wear amount (g)	0.1129	0.2174	0.4021	0.0058
Theoretical prediction error	−3.32%	−9.30%	−4.99%	3.57%
Simulated wear amount (g)	0.1127	0.2291	0.4011	0.0058
Simulated wear error	−3.51%	−4.42%	−5.22%	3.57%

4.2.5 Three-dimensional Topography and Wear Type

Images of all test conditions from the three-dimensional morphometer are shown in Figure 9. In order to show the morphological differences before and after wear more intuitively, one three-dimensional topography for each material is selected and presented in Figure 10. The top half of each subgraph represents the chosen three-dimensional picture, and the bottom half is the depth map where the ruler is placed. It reflects the depth corresponding to the ruler position in the top half. The observation position for topography on the test piece is set to where the left part is worn, and the right part is unworn, which is caused by the small deviation between the two test pieces. The circles in subgraphs show the depth of the observation position. It can be seen that the depth difference between the left and right parts is obvious.

It is widely accepted that according to the wear mechanism, wear can be divided into five basic types: adhesive wear, abrasive wear, fatigue wear, corrosion wear, and fretting wear. The wear phenomena of the five types of wear are as follows. For adhesive wear, material transfer should appear; for abrasive wear, surface scratches or furrow phenomena is the key phenomenon; for fatigue wear, pitting pits are formed on the worn surface; for corrosion wear, chemical reaction occurs at the contact interface, resulting in surface corrosion; for fretting wear, the wear area should be small. In our experiment, fatigue wear and fretting wear can be easily excluded. It can be seen from Figure 9 that due to the friction between the four viscoelastic materials and Q235, there is no furrow-like damage and no observed chemical damage on the

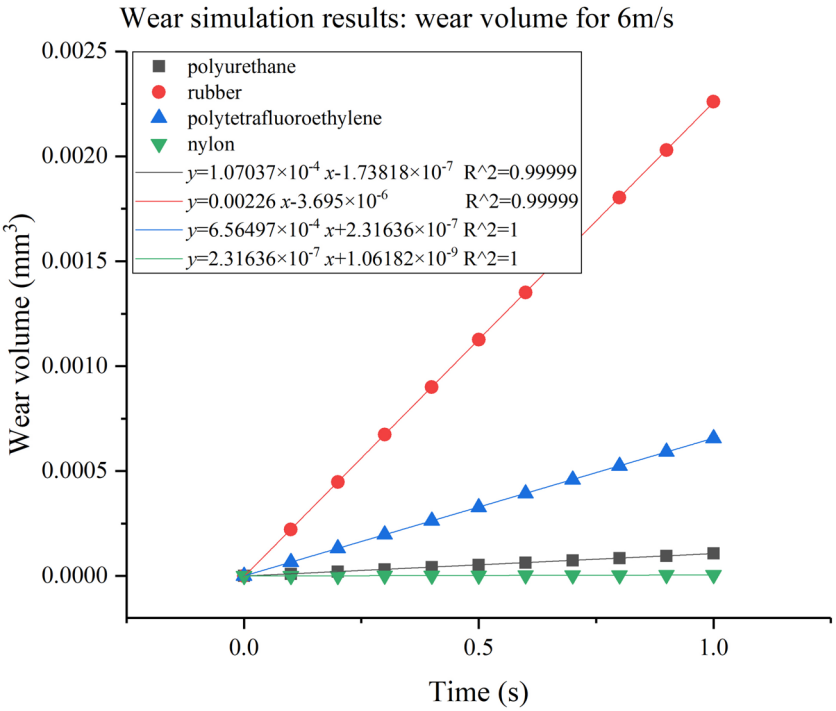

Figure 8 Wear simulation result: wear volume for 6 m/s

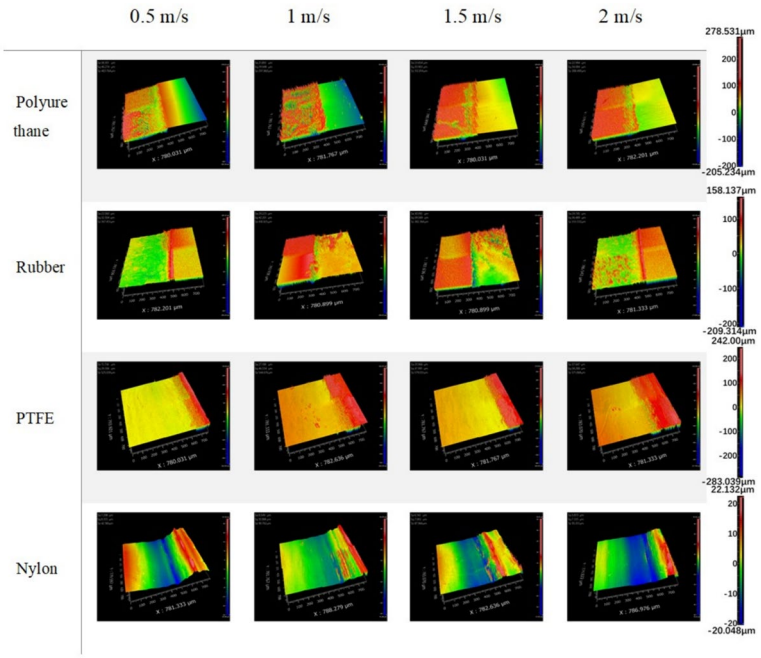

Figure 9 All three-dimensional topography pictures

surface. Besides, during the experiment, material transfer was observed, but due to centrifugal force, it fell on the test bench instead of staying on the test piece, which can be seen in Figure 1(c). Therefore, it is concluded that the wear type of the four materials against Q235 is

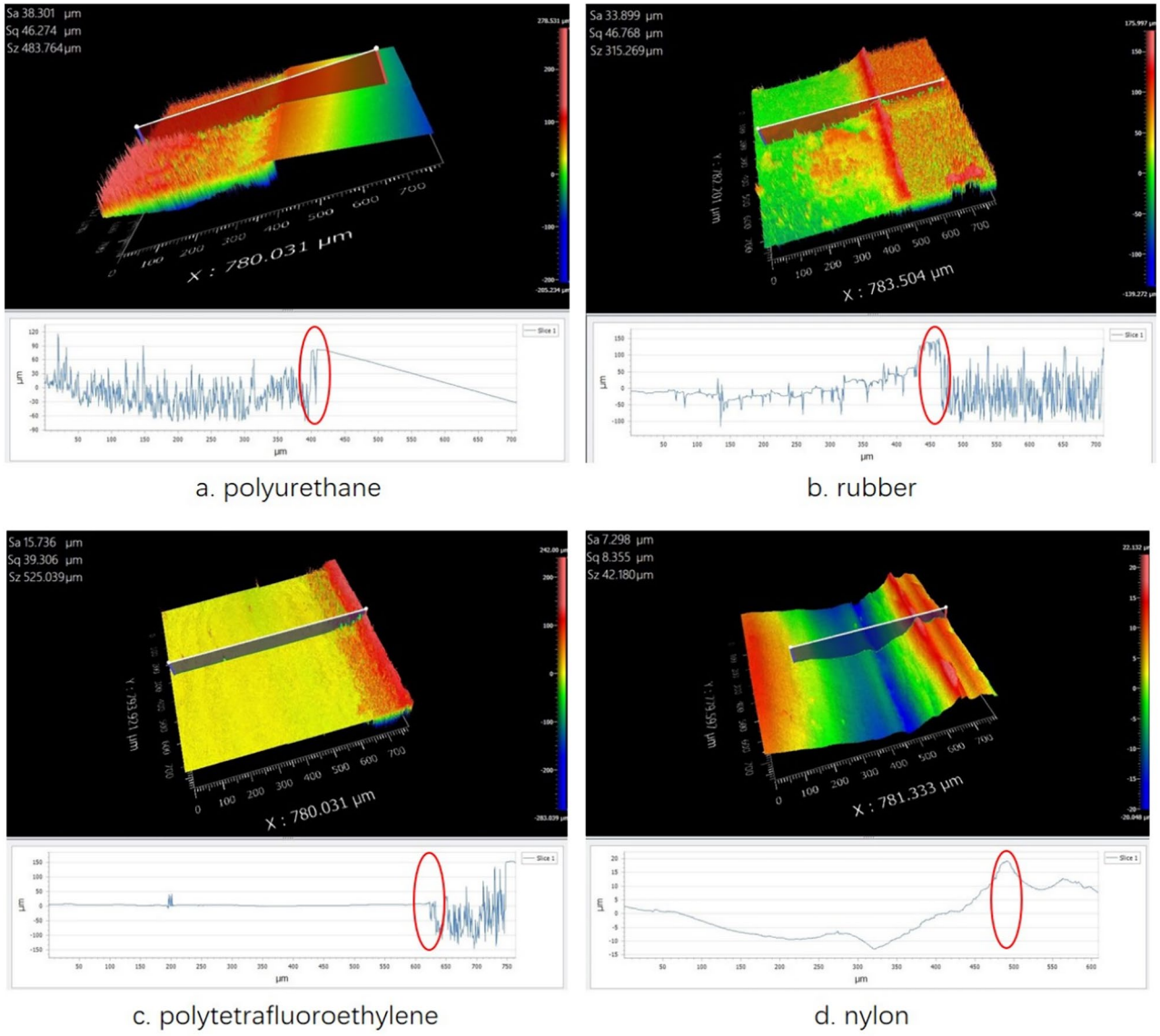

Figure 10 Three-dimensional topography selected to show details before and after wear for (**a**) polyurethane, (**b**) rubber, (**c**) PTFE, (**d**) nylon

adhesive wear, which provides support for the simulation assumption in Section 4.2.3.

As can be seen in the depth map for polyurethane and rubber materials (Figure 10(a) and (b)), the unworn area shows a sloping trend, which is caused by plastic deformation due to the force holding the test piece on the axis of rotation. Young's modulus of polyurethane and rubber is small, so the deformation caused by the same force is large. After a long time of deformation, this trend occurs. In addition, when looking at the depth maps of the worn and unworn areas, the surface roughness of the four materials varies after wear: the surface roughness of PTFE decreases after wear. The surface roughness of polyurethane increases and the surface roughness of rubber may increase or decrease after wear (see the circle in Figure 11), while the surface roughness of nylon remains almost unchanged after wear.

4.2.6 Guide Shoe Material Recommendation

In the comparison of the four materials, PTFE is found to exhibit relatively high sensitivity to speed and possess a larger Young's modulus, thus indicating its inferior shock absorption capabilities. Consequently, it is deemed unsuitable for high-speed applications and should be excluded from consideration. With regards to speed-index and velocity-wear factor, nylon emerges as the

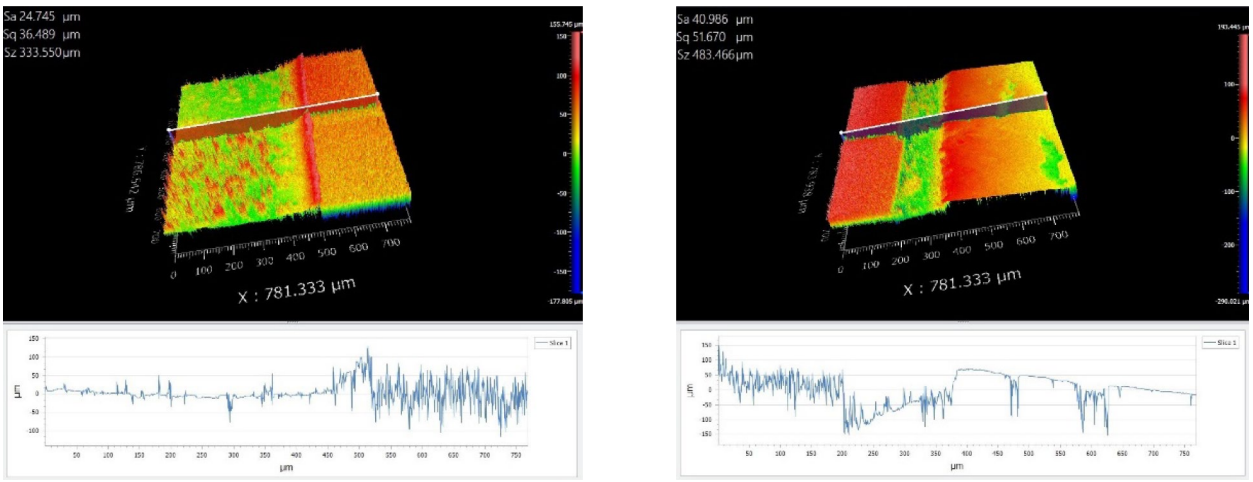

(a) surface roughness decreases (b) surface roughness increases

Figure 11 Two samples of three-dimensional topography of rubber show the different changes in surface roughness after wear: (**a**) surface roughness decreases, (**b**) surface roughness increases

superior material, exhibiting the lowest speed-index and velocity-wear factor. However, from the perspective of elevator comfort, nylon's excessive Young's modulus renders its shock absorption performance inferior to that of polyurethane and rubber. Therefore, in instances where the rails are in excellent condition, resulting in minimal vibration caused by uneven guide rails, nylon could be considered a viable option as a guide shoe material. Additionally, its reduced wear compared to other materials could effectively prolong the lifespan of the guide shoe. Nevertheless, when the condition of the guide rail cannot be guaranteed, polyurethane is highly recommended as the guide shoe material to ensure the utmost safety and comfort for users.

5 Conclusion and Outlook

The objective of this research is to investigate the wear model of viscoelastic materials. Based on the outcomes of experiments and simulations, the wear model for viscoelastic materials should be a modified version of the Archard model. According to the modified Archard wear model, various materials exhibit different sensitivities to velocity, depending on their respective speed-index. This implies that their wear performance under high-speed conditions can vary significantly. By comparing and analyzing the measured wear amounts, the following conclusions are drawn:

(1) The speed-index of polyurethane, rubber, PTFE, and nylon are 0.5735, 3.0918, 1.6966, and 0.3338, respectively. These values indicate that polyurethane and nylon are less sensitive to speed, while rubber and PTFE are more sensitive to speed, providing effective support for wear prediction.

(2) The wear prediction results of both theoretical derivation and simulation for the four materials are effective, and the errors are within acceptable range. Therefore, it is considered that the modified Archard wear model can be used for wear prediction under high-speed conditions. Furthermore, the model also provides support for the selection of guide shoe materials under high-speed conditions.

(3) The velocity-wear factors of polyurethane, rubber, PTFE, and nylon are 3.2238×10^{-6}, 4.3479×10^{-5}, 2.6817×10^{-6}, and 3.0147×10^{-8}, respectively. This indicates that the rubber material wears out fastest in the friction process and nylon the slowest, which provides guidance for the selection of guide shoe materials.

(4) It is recommended that the selection between nylon and polyurethane as guide shoe material should depend on actual situations. From the experiment results, nylon has the smallest speed-index and the smallest velocity-wear factor, which makes its wear rate the lowest. However, from the perspective of elevator comfort, the larger Young's modulus makes nylon perform poorer than polyurethane in shock absorption. As a result, when the flatness of guide rail can be guaranteed, despite its deficient performance in shock absorption, nylon could be considered as a guide shoe material. However, when the guide rail's flatness cannot be guaranteed, polyurethane is recommended as the guide shoe material to ensure users' safety and comfort.

In summary, this research has delved into the wear model of viscoelastic materials, specifically exploring the speed-index of four distinct materials. Based on this wear model, higher-speed wear simulations and experimental validations have been conducted. The results obtained indicate that this model can effectively predict wear under higher-speed conditions. It is noteworthy, however, that the wear processes and mechanisms involved in rolling contact between viscoelastic and metallic materials remain beyond the scope of this study. As we proceed with future research, it would be intriguing to investigate these wear mechanisms further by comparing simulated surfaces with experimental results, particularly those represented in three-dimensional maps. Such an approach would afford a deeper understanding of the intricate interactions and wear behaviors that occur during rolling contact.

Acknowledgments
Not applicable.

Author Contributions
LC was in charge of the whole study, carried out the research, and wrote the manuscript; LY prepared research resources and assisted in validation; CL and ZZ provided theoretical guidance and revised the manuscript. All authors read and approved the final manuscript.

Funding
Supported by National Natural Science Foundation of China(Grant No. 51935007).

Availability of Data and Materials
The datasets used and/or analyzed during the current study are available from the corresponding author on reasonable request.

Declarations

Competing Interests
The authors declare that they have no competing interests.

Received: 26 July 2023 Revised: 21 June 2024 Accepted: 24 June 2024
Published online: 15 July 2024

References

[1] D Mei, X Du, Z Chen. Vibration analysis of high-speed traction elevator based on guide roller-rail contact model. *Journal of Mechanical Engineering*, 2009, 45(5): 264-270.
[2] R Zhang, C Wang, Q Zhang. Response analysis of the composite random vibration of a high-speed elevator considering the nonlinearity of guide shoe. *Journal of the Brazilian Society of Mechanical Sciences and Engineering*, 2018, 40: 1-10.
[3] C Chen, R Zhang, Q Zhang, et al. Mixed H2/H∞ guaranteed cost control for high speed elevator active guide shoe with parametric uncertainties. *Mechanics & Industry*, 2020, 21(5): 502.
[4] R Tao, Y Xu, F Deng, et al. Feature extraction of an elevator guide shoe vibration signal based on SVD optimizing LMD. *Journal of Vibration and Shock*, 2017,36(22): 166-171.
[5] S Zhang, R Zhang, Q He, et al. The analysis of the structural parameters on dynamic characteristics of the guide rail–guide shoe–car coupling system. *Archive of Applied Mechanics*, 2018, 88: 2071-2080.
[6] G Qin, Z Yang. Time-varying characteristics of guide roller-rail contact stiffness of super high-speed elevator under aerodynamic load. *Journal of the Brazilian Society of Mechanical Sciences and Engineering*, 2021, 43: 1-14.
[7] Y Liu, T W Liskiewicz, B D Beake. Dynamic changes of mechanical properties induced by friction in the Archard wear model. *Wear*, 2019, 428: 366-375.
[8] H Wang, C Zhou, Y Lei, et al. An adhesive wear model for helical gears in line-contact mixed elastohydrodynamic lubrication. *Wear*, 2019, 426: 896-909.
[9] B Liu, S Bruni, R Lewis. Numerical calculation of wear in rolling contact based on the Archard equation: Effect of contact parameters and consideration of uncertainties. *Wear*, 2022, 490: 204188.
[10] C Zhang, G Zhao, T Li, et al. An investigation of die wear behavior during aluminum alloy 7075 tube extrusion. *Journal of Tribology*, 2013, 135(1): 011602.
[11] X Liao, Y Chen. Research on the wear life of slipper in aero-hydraulic pump based on Archard wear model and liquid friction work. *2013 International Conference on Quality, Reliability, Risk, Maintenance, and Safety Engineering (QR2MSE)*, 2013: 930-934.
[12] G Yu, W Xia, Z Song, et al. Wear-life analysis of deep groove ball bearings based on Archard wear theory. *Journal of Mechanical Science and Technology*, 2018, 32: 3329-3336.
[13] Ansys Help: Mechanical APDL 2023 R1. *Contact technology guide, including wear in a contact analysis*. Canonsburg, PA: ANSYS, Inc., 2023[2023-07-07]. https://ansyshelp.ansys.com/account/secured?returnurl=/Views/Secured/corp/v231/en/ans_ctec/ctec_includwear.html.
[14] S Naderizadeh, A Athanassiou, I S Bayer. Interfacing superhydrophobic silica nanoparticle films with graphene and thermoplastic polyurethane for wear/abrasion resistance. *Journal of Colloid and Interface Science*, 2018, 519: 285-295.
[15] R Zhou, D H Lu, Y H Jiang, et al. Mechanical properties and erosion wear resistance of polyurethane matrix composites. *Wear*, 2005, 259(1-6): 676-683.
[16] S Xiao, H J Sue. Effect of molecular weight on scratch and abrasive wear behaviors of thermoplastic polyurethane elastomers. *Polymer*, 2019, 169: 124-130.
[17] T Nishi. Rubber wear mechanism discussion based on the relationship between the wear resistance and the tear resistance with consideration of the strain rate effect. *Wear*, 2019, 426: 37-48.
[18] Q He, Y Zhou, W Qu, et al. Wear property improvement by short carbon fiber as enhancer for rubber compound. *Polymer Testing*, 2019, 77: 105879.
[19] Z Zheng, H Yang, X Yao. Wear-resistant graphene–silicone rubber composites. *Tribology Transactions*, 2020, 63(2): 205-214.
[20] W Sun, X Liu, K Liu, et al. Mechanochemical functionality of graphene additives in ultralow wear polytetrafluoroethylene composites. *Carbon*, 2021, 184: 312-321.
[21] L F Tóth, P De Baets, G Szebényi. Thermal, viscoelastic, mechanical and wear behaviour of nanoparticle filled polytetrafluoroethylene: a comparison. *Polymers*, 2020, 12(9): 1940.
[22] W Sun, J Ye, X Liu, et al. Atomistic insights into anti-wear mechanisms and protective tribofilm formation in polytetrafluoroethylene composites. *Journal of Tribology*, 2022, 144(9): 091701.
[23] S Sudhagar, V M Raja, S S Kumar, et al. The wear behavior and service life of Madar and Bauhinia Racemosa reinforced polyester hybrid composites for gear applications. *Materials Today: Proceedings*, 2019, 19: 589-593.
[24] S Huang, B Pan, M Xie, et al. Synergistic effects of graphene oxide and paraffin wax on the tribological properties of monomer casting nylon-6 composites. *Tribology International*, 2021, 154: 106726.
[25] B Lin, A Wang, T Sui, et al. Friction and wear resistance of polytetrafluoroethylene-based composites reinforced with ceramic particles under aqueous environment. *Surface Topography: Metrology and Properties*, 2020, 8(1): 015006.
[26] M Shen, B Rong, Q Li, et al. Different responses of the wheel-rail interface adhesion and wheel surface damage induced by an out–of–round wheel tread. *Wear*, 2023, 526: 204956.
[27] M Shen, J Li, L Li, et al. Adhesion and damage behaviour of wheel–rail rolling–sliding contact suffering intermittent airflow with different humidities and ambient temperatures. *Tribology Letters*, 2024, 72(1): 18.

[28] Q Wu, T Qin, M Shen, et al. Effect of gas nitriding on interface adhesion and surface damage of CL60 railway wheels under rolling contact conditions. *Metals*, 2020, 10(7): 911.
[29] J A Williams. Wear and wear particles—some fundamentals. *Tribology International*, 2005, 38(10): 863-870.
[30] D Kim, L Quagliato, D Park, et al. Lifetime prediction of linear slide rails based on surface abrasion and rolling contact fatigue-induced damage. *Wear*, 2019, 420: 184-194.
[31] M Akama, T Kimata. Numerical simulation model for the competition between short crack propagation and wear in the wheel tread. *Wear*, 2020, 448: 203205.
[32] A Ramalho, M Esteves, P Marta. Friction and wear behaviour of rolling–sliding steel contacts. *Wear*, 2013, 302(1-2): 1468-1480.
[33] I Khader, D Kürten, A Kailer. A study on the wear of silicon nitride in rolling–sliding contact. *Wear*, 2012, 296(1-2): 630-637.
[34] C Zhou, S Ren, H Feng, et al. A new model for the preload degradation of linear rolling guide. *Wear*, 2021, 482: 203963.

Longye Chen born in 1994, is currently a PhD candidate at *School of Mechanical Engineering, Shanghai Jiao Tong University, China*. He received the M.Sc. in mechanical engineering from *Tufts University, USA,* and *the Hong Kong Polytechnic University, China*. His main research interests include rolling friction and viscoelastic material.

Lingyu Yan born in 1978, is currently a PhD candidate at *School of Mechanical Engineering, Shanghai Jiao Tong University, China*. He received the M.Sc. in mechanical engineering from *Shanghai Jiao Tong University, China*. His main research interests include hoistway aerodynamics and elevator car shape design.

Chengliang Liu born in 1964, received the PhD degree in mechanical engineering from *Southeast University, China*, in 1999. He is currently a Chair Professor at *School of Mechanical Engineering, Shanghai Jiao Tong University, China*. His main research interests include machine health and intelligent operations, fluid transmission and control, and intelligent sensing and mechatronic fusion design.

Zhinan Zhang born in 1978, received the PhD degree in mechanical engineering from *Shanghai Jiao Tong University, China*, in 2011. He is currently a Professor at *School of Mechanical Engineering, Shanghai Jiao Tong University, China*. His main research interests include computational design and analysis of tribosystems, tribo-informatics, and design theory and methods of design engineering and innovation.